Topological Optimization of Under-Platform Dampers With Moving Morphable Components and Global Optimization Algorithm for Nonlinear Frequency Response

E. Denimal
Department of Mechanical Engineering,
Imperial College London,
London SW7 2AZ, UK
e-mail: e.denimal@imperial.ac.uk

F. El Haddad
Department of Mechanical Engineering,
Imperial College London,
London SW7 2AZ, UK
e-mail: f.el-haddad@imperial.ac.uk

C. Wong
Rolls-Royce plc,
Derby DE2 48J, UK
e-mail: chian.wong@rolls-royce.com

L. Salles
Department of Mechanical Engineering,
Imperial College London,
London SW7 2AZ, UK

To limit the risk of high cycle fatigue, underplatform dampers (UDPs) are traditionally used in aircraft engines to control the level of vibration. Many studies demonstrate the impact of the geometry of the damper on its efficiency, thus the consideration of topological optimization (TO) to find the best layout of the damper seems natural. Because of the nonlinear behavior of the structure due to the friction contact interface, classical methods of TO are not usable. This study proposes to optimize the layout of an UDP to reduce the level of nonlinear vibrations computed with the multiharmonic balance method (MHBM). The approach of TO employed is based on the moving morphable components (MMC) framework together with the Kriging and the efficient global optimization algorithm to solve the optimization problem. The results show that the level of vibration of the structure can be reduced to 30% and allow for the identification of different efficient geometries. [DOI: 10.1115/1.4049666]

Introduction

In the aerospace industry, the requirements for the design of engines are becoming more stringent and new engines must be more efficient and lighter. Thus, each component tends to reach its structural limits. Considering the turbine blades, they are submitted to high level of exposure to thermal stresses, centrifugal stresses, or vibrational stresses [1,2]. The latter can lead to high cycle fatigue and can potentially lead to a failure of the blades [3]. Because of the large operating speed range and the high modal density of bladed disks, all the critical resonances cannot be avoided. For this reason, it is crucial to limit the level of vibrations at resonance. The most widely used solution are based on friction damping [4–6].

Dry friction can be introduced in different locations of the structure (shrouds, roots, blade tips), but the most efficient solution relies on the use of underplatform dampers (UPDs) [6,7]. They are located in the groove under the platforms of two adjacent blades and consist in a small metal device. They remain in contact with the platforms due to the centrifugal loading. When the blades vibrate, the relative displacement between the platforms and the UPD generates friction and so energy is dissipated [8,9].

The geometry of the UPD has a significant impact on its effectiveness. Indeed, many studies are related to the study of the comparison of different geometries. The most classical geometries are based on a wedge geometry [10–12], a cylindrical geometry [11,13] or a mix of them [14]. From those studies, it appears that the shape and the geometry of the damper has a high impact on its efficiency.

Topological optimization (TO) for continuum structures consists in the identification of a subdomain occupied by the structure in a total available domain where only the boundary conditions are known [15,16]. The topology of a component is defined by its internal and external boundaries and by the number of inner holes. These characteristics are optimized simultaneously with respect to a predefined objective and constraint functions. TO is mostly used in a predesign stage to identify the most efficient layout of the structure. The two most classical methods of TO are the density-based approach and the level set method. The first method consists in the optimization of the element densities of a mesh describing the design space [17,18]. The second one is based on an implicit description of the material boundaries with a level set function (LSF), which is often propagated by solving a Hamilton–Jacobi equation [19,20]. These two approaches require the sensitivities, of the densities or of the shape, with respect to the objective function and the constraints. These sensitivities might be impossible to determine analytically for some problems and are too expensive to be determined numerically.

A recent approach, called the moving morphable components (MMC) framework, was proposed by Guo et al. [21]. The basic idea relies on the fact that the topology can be described by the association of elementary beams. Hence, the material domain is still described by an LSF which is decomposed in local LSFs that describe each beam. The expression of these local LSF is explicit and depends on a few parameters. Hence, the size of the optimization problem is drastically reduced, and it gives the opportunity to consider global optimization methods. Thus, in 2019, Raponi et al. [22] proposed to use the Kriging metamodeling method together with the efficient global optimization (EGO) algorithm [23] to solve a problem of topological optimization for crashworthiness where the sensitivities cannot be determined.

Considering vibration issues, TO has been applied to the optimization of eigenvalues in a linear context in Ref. [24–27] with the different methods presented previously. The extension to the nonlinear case is done in Refs. [28] and [29] where the width of a clamped–clamped beam is optimized (constant thickness) and geometric nonlinearities are considered. Gradient-based optimization is used for the optimization. Considering contact problems, the problem of TO has been addressed in a quasi-static context in Refs. [30–32]. The objective of this study is to perform TO for the optimization of nonlinear dynamic systems in the presence of a friction interface, which has never been done before according to the best of our knowledge. Here, TO is applied on a UPD to

identify the damper's layout that reduces to the maximum the levels of the nonlinear vibrations of the blades on a given frequency range. The optimization process must take into consideration the friction contact interface between the damper and the structure, but also the fact that the load applied on the UPD depends on its mass, and so on its geometry. Furthermore, the objective function of the problem is expected to be strongly nonconvex with many local minima. For this reason, global optimization is considered and the MMC framework with Kriging-based optimization is used to solve the current problem.

The objective of this paper is to investigate the capacity of the MMC framework coupled with global optimization algorithm to optimize the topology of an UPD in order to reduce the amplitude of the nonlinear vibrations of the blades. Hence, the methodology is applied on a two-dimensional (2D) system that simulates the behavior of a real high pressure turbine blade as a preliminary work to examine the potential of the approach. This paper is organized as follows: first, the optimization problem is introduced. The mechanical system, the problem geometry, and the methodology used to determine the nonlinear vibrations of the structure are presented. Second, the MMC framework and the optimization process based on Kriging and on the EGO algorithm are presented. Finally, the numerical results are presented.

Problem Presentation

The objective of this section is to present the physical problem that will be optimized. Hence, the mechanical system as well as the modeling choices and the numerical strategy for the prediction of the nonlinear vibrations are presented.

Model Presentation. The model used is based on the geometry of an underplatform test rig used and presented in Ref. [12]. It was designed to simulate the dynamic behavior of the dynamic response of a real high pressure turbine blade and to study the impact of UPD on a blade-like structure. The model considered here is based on the 2D geometry of this structure and is represented Fig. 1. It is composed of two pseudo-beams fixed on a common base which simulates a rigid disk. To be consistent with the work done before in Ref. [12], the boundary conditions remain the same and the right side of the base is clamped for later experimental validations. A 2D geometry may seems simplistic, but the main concern of this study is to investigate the interest and the possibilities of using Kriging-based optimization for TO of nonlinear vibrations with friction. This simple case allows for much lower simulation times and a lower number of optimization parameters.

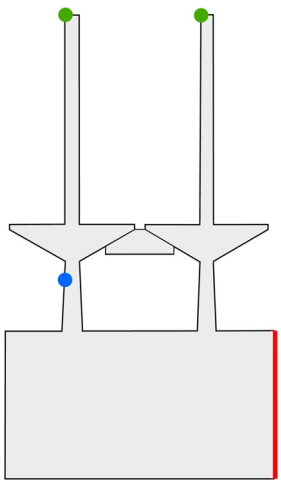

Fig. 1 Two-dimensional geometry of the model: (—) clamped, (●) excitation point, and (●) output points

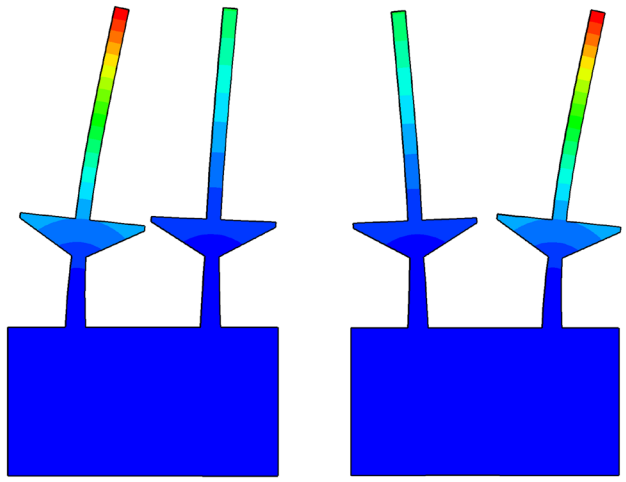

Fig. 2 First two modes of the structure without the damper: (*a*) in-phase mode: $f_1 = 246.73$ Hz and (*b*) out-of-phase mode: $f_2 = 247.51$ Hz

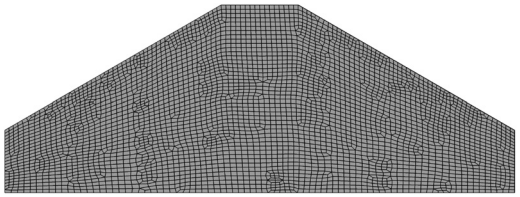

Fig. 3 Mesh of the full damper

The mesh of the blades is composed of 3324 eight-node biquadratic plane strain elements. The structure is made of steel with a Young modulus of 197 GPa and a density equal to 7800 kg/m^3. The study focuses on the first bending mode of the blades. As there are two blades, their motion can be in-phase or out-of-phase. These two modes are represented in Fig. 2, and the natural frequencies are equal to 246.73 Hz and 247.51 Hz, respectively. It is worth noticing that they are determined without the damper.

As a reference case, a wedge damper is located between the two platforms of the blades as represented in Fig. 1. The centrifugal loading keeps it in place during operation. The mesh of the damper is represented in Fig. 3 and is composed of 3604 eight-node biquadratic plane strain elements. The mesh is constructed so that the contact points between the damper and the blades are matching. The number of elements may seem huge for this component, but this mesh will be used later in the process of the topological optimization and corresponds to the discretization of the problem.

A node-to-node contact formulation is used in the problem, and 51 contact points are present on each side of the damper. The dynamic behavior at each contact node is modeled with a one-dimensional friction contact element. It consists of one Jenkins element and one other spring to allow normal load variations. Each element is characterized by four parameters, namely, the friction coefficient, μ; the tangential stiffness, k_t; the normal stiffness, k_n; and the initial preload, N_0. The normal preload and the stiffness are normalized by unit of area, so each contact element has its own characteristics. During the cycle, the normal loading is kept constant and no separation is possible.

The contact pressure due to the centrifugal loading C_F is modeled by a constant value [10], and the initial pressure σ_0 on each side of the damper is given by

$$\sigma_0 = \frac{1}{2}\frac{C_F}{A(\cos\alpha + \mu\sin\alpha)} \tag{1}$$

where A is the contact area on each side, μ is the friction coefficient, and α is the damper angle. The load C_F, aimed to simulate the centrifugal loading, is given by $C_F = m_{\text{damper}} \times R \times \omega^2$, where m_{damper} is the damper mass, R is the radius, and ω is the rotational speed.

Multiharmonic Balance Method. The friction interface brings nonlinearity in the system, and specific numerical strategies must be employed to determine the vibration levels. Thus, the method of the multiharmonics balance (MHBM) coupled with a model reduction technique included in the in-house code FORSE (FORce Response SuitE) is used in this study. The latter has been presented in detail in Refs. [33] and [34]. The reduction of the model is based on a frequency response function (FRF) matrix representation of the model. This FRF matrix is determined by calculating its exact value at some frequency points and adding a second term that describes its variation in a range of frequencies [34].

The dynamic equation of the system can be written as

$$\mathbf{M}\ddot{\mathbf{u}} + \mathbf{C}\dot{\mathbf{u}} + \mathbf{K}\mathbf{u} + \mathbf{f}_{nl}(\mathbf{u}, \dot{\mathbf{u}}) = \mathbf{p}(t) \tag{2}$$

where $\mathbf{M}$, $\mathbf{C}$, and $\mathbf{K}$ are the mass, damping, and stiffness matrices, respectively. $\mathbf{f}_{nl}$ corresponds to the nonlinear forces vector due to the friction contact, $\mathbf{p}$ is the external forces vector, and $\mathbf{u}$ is the displacements vector. The dot represents the derivative with respect to the time. As the external forces are periodic, it is natural to search for a periodic response for Eq. (2). Hence, the idea of the MHBM is to write the problem on a Fourier series composed of N_h retained harmonics. So the response can be written as

$$\mathbf{q}(t) = \mathbf{q}_0 + \sum_{i=1}^{N_h} \mathbf{q}_i^C \cos(k_i \omega t) + \mathbf{q}_i^S \sin(k_i \omega t) \tag{3}$$

where $\mathbf{q}_0$ is the constant term in the Fourier series, $\mathbf{q}_i^C$ are the cosine coefficients, $\mathbf{q}_i^S$ are the sine coefficients, and k_i is the ith retained harmonic. The harmonics retained are chosen a priori by the user. By injecting the latter in Eq. (2), and using the orthogonality of the Fourier series, the problem can be approximated by

$$\mathbf{Z}(\omega)\tilde{\mathbf{q}} + \tilde{\mathbf{f}}_{nl} = \tilde{\mathbf{p}} \tag{4}$$

where $\mathbf{Z}$ is the dynamic stiffness matrix, $\tilde{\mathbf{q}} = \{\mathbf{q}_0, \mathbf{q}_1^C, \mathbf{q}_1^S, \ldots, \mathbf{q}_n^C, \mathbf{q}_n^S\}$ is the vector of the Fourier coefficients, and $\tilde{\mathbf{f}}_{nl}$ and $\tilde{\mathbf{p}}$ are the nonlinear and the external efforts expressed in the Fourier basis, respectively. An AFT algorithm is used for the determination of the nonlinear forces Fourier coefficients [35]. Problem (4) is solved by using a Newton–Raphson algorithm. To find a continuous response curve with regard to the pulsation of excitation ω, continuation is used. Here, a secant predictor together with an arc-length corrector is used. In the following of the paper, harmonics 1 and 3 are retained for the MHBM simulations. This choice is based on a convergence study, not presented here for the sake of consistency.

Application on the Initial Test Case. The method of the MHBM is then used to compute the nonlinear dynamic response of the structure. The system is excited at the bottom of the left blade (see Fig. 1), and the displacements at the blades tips are determined (green points in Fig. 1). A friction coefficient equal to 0.5 is chosen, and the contact stiffness are taken equal to $k_t = k_n = 0.5$ N/mm^3. Different excitation levels are considered from 1×10^{-5} to 1×10^{-2} N, and the nonlinear receptances of the point at the tip of the left blade are given in Fig. 4. For the full damper, the centrifugal loading C_F is equal to 9.54×10^{-4} N.

For excitation force equal to 1×10^{-5} N or 1×10^{-4} N, two resonant frequencies appear at 246.6 Hz and 248.6 Hz (curves superimposed in Fig. 4). When the excitation force increases to

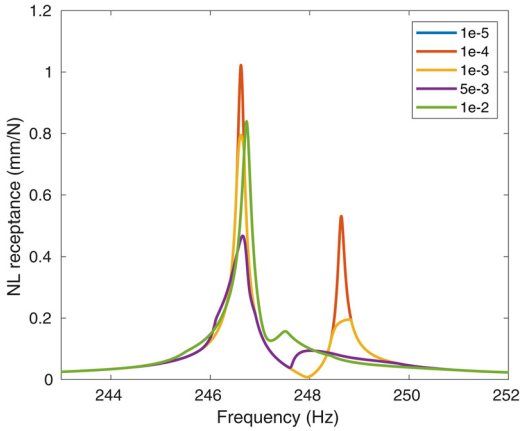

Fig. 4 Nonlinear receptance at the point on the left blade for different excitation levels for a full damper

1×10^{-3} N, a damping effect appears, and the two peaks are cut. If the excitation force is increased to 5×10^{-3} N, the two peaks are even more damped, but the second peak is shifted to 248 Hz. Finally, if the excitation force is again increased to 1×10^{-2} N, the receptance for the first peak increases and the resonant frequency is slightly shifted of 0.1 Hz. For the second peak, the resonant frequency continues to be shifted and is equal to 247.5 Hz and the receptance also increases.

Optimization Problem. The objective is to optimize the topology of the damper in order to identify the geometry that gives the minimum level of vibrations at blade tips. Thus, the maximum of vibration amplitudes observed at blades tips over the frequency range $[100, 400]$ Hz is chosen as the objective function of the problem. The frequency range is chosen in order to cover all the possible variation of the resonance frequencies that may happen during the optimization problem and to ensure a good initialization of the MHBM. The limits of the design space are the limits of the full damper presented in Fig. 3. The excitation amplitude is fixed to 1×10^{-3} N and is constant during the whole study. The loading range is directly related to the damper mass and can take value between 0 N (damper of null mass) and 9.54×10^{-4} N (full damper).

Moving Morphable Components Framework and Optimization Process

The objective of this section is to present the methodology employed to perform topological optimization. The methodology is based on the Kriging-Level Set Method [22]; in other words, the structure is represented implicitly by a LSF. The Kriging is used to surrogate this LSF and to update it to identify the best layout.

Parametrization of the Problem. Let us consider a bounded domain $\mathscr{D} \in \mathbb{R}^2$ which is the domain of all the admissible shapes. Ω denotes the region of the domain $\mathscr{D}$ occupied by the material. The LSF Φ that describes Ω is defined as

$$\begin{cases} \Phi(\mathbf{v}) > 0, & \mathbf{v} \in \Omega \\ \Phi(\mathbf{v}) = 0, & \mathbf{v} \in \delta\Omega \\ \Phi(\mathbf{v}) < 0, & \mathbf{v} \in D \backslash \Omega \end{cases} \tag{5}$$

where $\mathbf{v} = (x, y)^{\mathrm{T}} \in \mathscr{D}$ is a point of the domain and $\delta\Omega$ is the interface between the material and void. The 0-isoline defines precisely the limit between material and void.

The idea of the MMC framework proposed by Guo et al. [21] is to decompose this global LSF into several local LSFs that

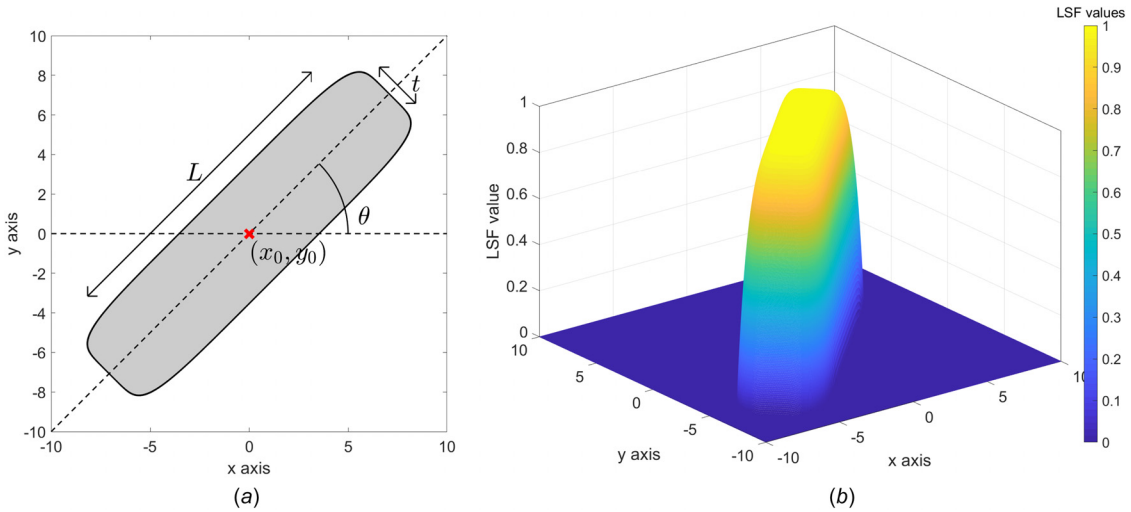

Fig. 5 (*a*) Parameterization of a component and (*b*) corresponding LSF

describe an elementary beam component which can be moved and deformed in the design space. The idea relies on the fact that the optimal topologies can often be decomposed in an ensemble of interconnected beams. Hence, each local LSF Φ_i describes a domain Ω_i occupied by the component i. The total domain Ω occupied is defined by $\Omega = \cup_{i=1}^{N} \Omega_i$.

For $\mathscr{D} = \mathbb{R}^2$, each component i is described by an explicit formulation of the LSF given by [21]

$$\Phi_i(\mathbf{u}) = -\left[\left(\frac{\cos\theta_i(x - x_{0i}) + \sin\theta_i(y - y_{0i})}{l_i/2} \right)^m + \left(\frac{-\sin\theta_i(x - x_{0i}) + \cos\theta_i(y - y_{0i})}{t_i/2} \right)^m - 1 \right] \tag{6}$$

where (x_{0i}, y_{0i}) is the center position of the component, θ_i is the inclination angle, L is the length, and t is the thickness. m is a relatively large even number taken equal to 6 here, as defined in Ref. [21]. Hence, each component is described by a set of five parameters, namely, $(x_{0i}, y_{0i}, \theta_i, L, t)$, as illustrated in Fig. 5 where the parameterization of a component is displayed. The corresponding local LSF is given in Fig. 5(*b*), where the negative values have been set to zero for display considerations. By changing these five parameters, each component can move and be distorted, and the assembly of the different components describes the general structure.

Once the structure is described by the LSF, this description must be mapped on the mechanical model and more precisely on the mesh. A classical method consists in having a fixed mesh on which the LSF is mapped with the use of an ersatz material: for the regions occupied by the material, the density of the material are used, but for the region composed of void, an ersatz material is used (i.e., with a density and a Young modulus largely lower than the material used). This allows to work on a fixed mesh and to always have a well-defined mechanical problem. This approach is largely used in the community [19–22,36]. However, in the computation of the eigenmodes of a structure, some can be localized in the ersatz material. To avoid this problem, the void elements are removed [37]. Hence, in this study, the elements of the mesh that are not occupied by the material are removed. Moreover, the LSF is discretized in the center of the elements [36], i.e., if the LSF is positive at the center of an element of the mesh, then this element is composed of material, but if the LSF is negative, then the element is removed. This discretization might seem a bit coarse; however, the mesh can be refined (without additional numerical cost) for a more accurate description of the geometry of the damper. A second argument is that the topological optimization process is used to identify types of geometries that might be more efficient, but other design considerations need to be considered after and will define the final layout. To ensure a realizable component, the connectivity of the component is first checked with a 2D graph as proposed by Raponi et al. [22], and if checkboard effect takes place, then the thickness of the components is increased. An example of the global process is illustrated in Fig. 6, where in Fig. 6(*a*), a 2D graph is given. Each component is reduced to a segment and is represented by a color. The limits of the design space are given in black. In Fig. 6(*b*), the 0-isocontour of each LSF is represented, and finally, the corresponding mesh is represented in Fig. 6(*c*).

Optimization With Kriging and Efficient Global Optimization Algorithm. The optimization problem considered in this paper can be written in the following form:

$$\min_{\mathbf{x}} f_{\text{obj}}(\mathbf{x}) \tag{7}$$

where f_{obj} is the objective function of the problem, namely, the maximum of displacements at the blades tips. $\mathbf{x} \in \mathbb{R}^n$ is the vector of the design parameters that describe the geometry of the problem, which, in this case, corresponds to the number of LSF used multiplied by 5, which are the describing parameters. The optimization problem is written without a constraint on the volume of the damper. This choice is driven by the fact that the most important goal in this study is to get a more efficient geometry, than a lighter one. Hence, no volume constraint is considered as it could lead to missing of some efficient geometries.

The problem considered is strongly nonlinear, nonconvex with many local minima, and the determination of the shape sensitivities of the objective function is not conceivable. Hence, an optimization strategy based on global optimization is considered. More precisely, the methodology is based on the use of a Kriging metamodel together with the EGO algorithm [23].

Kriging Surrogate Model. Kriging is an approach to surrogate a function that is often expensive to compute. In the present case, it surrogates the objective function f_{obj}. It is based on a set of N inputs $\mathbf{X} = \{\mathbf{x}^{(1)}, \ldots, \mathbf{x}^{(N)}\}$ and their evaluations $\mathbf{y} = \{y^{(1)}, \ldots, y^{(N)}\}$. In the present case, each $y^{(k)}$ is obtained by computing the displacements FRF at blades tips with the MHBM, considering the damper geometry described by $\mathbf{X}^{(k)}$ over the frequency range [100, 400] Hz. The maximum over the frequency range and over the two blades is taken as the evaluation of the

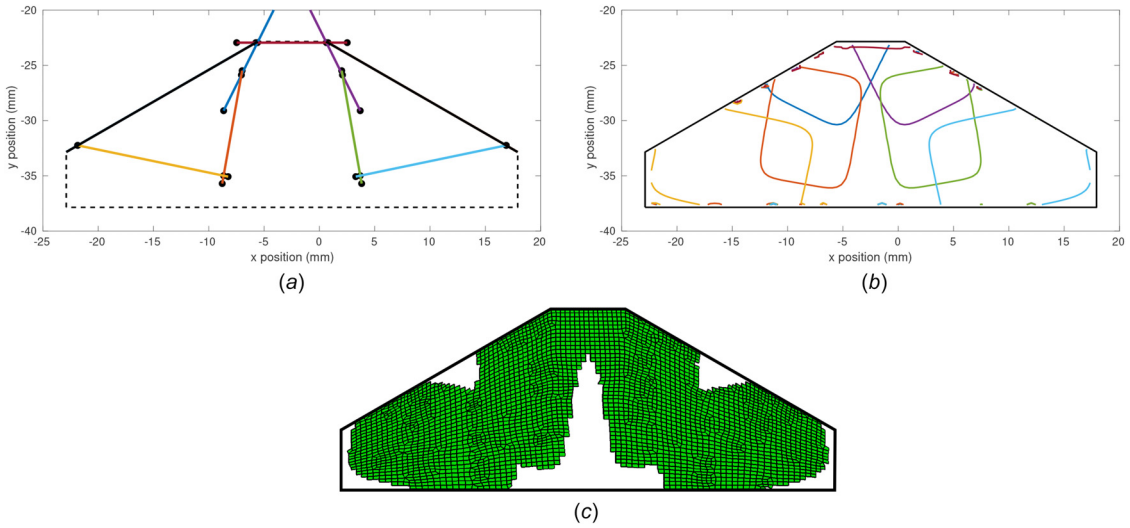

Fig. 6 General geometry description: (*a*) 2D graph for the connectivity check, (*b*) 0-isocontour of the different LSF, and (*c*) corresponding mesh

objective function. This set of inputs and outputs is called design of experiments (DoE). The set of input points is generated with a Latin hypercube sampling (LHS) and only the configurations that are connected and retained. Then, the Kriging methodology consists in approximating the function f_{obj} by the function $\hat{f}$ defined as [38]

$$\hat{f}(\mathbf{x}) = \sum_{j=1}^{q} g_j(\mathbf{x})\boldsymbol{\beta}_j + \mathscr{Z}(\mathbf{x}) \tag{8}$$

where $(g_j)_{j\in[1,q]}$ is a set of q known real-values functions, $(\beta_j)_{j\in[1,q]}$ are the regression coefficients to be determined, and $\mathscr{Z}$ is a stationary zero-mean Gaussian process. Its covariance function is given by $C(\mathbf{x},\mathbf{x}') = \sigma^2\mathscr{R}(\mathbf{x},\mathbf{x}')$, where σ^2 is the unknown variance of the process and $\mathscr{R}(\mathbf{x},\mathbf{x}')$ is the correlation function of the process. The functions $(g_j)_{j\in[1,q]}$ are chosen according to an a priori knowledge of the phenomenon, and they are often low order polynomial functions. The function $\mathscr{R}$ is usually unknown but is often constructed from a family of kernel functions parameterized by a parameter $\boldsymbol{\theta}$ to be optimized [38].

By assuming that $\mathscr{Z}$ is a Gaussian process, then the best unbiased predictor is linear. One can then define the regression matrix $\mathbf{G}$ of coefficients $G_{ij} = g_j(\mathbf{x}^{(i)})$ and the correlation matrix $\mathbf{R}$ of coefficients $R_{ij} = C(\mathbf{x}^{(i)},\mathbf{x}^{(j)})$. The prediction y_0 of the Kriging metamodel at the point $\mathbf{x}_0$ is then given by

$$y_0 = \hat{f}(\mathbf{X}_0) = \mathbf{g}_0^{\mathrm{T}}\tilde{\boldsymbol{\beta}} + \mathbf{r}_0^{\mathrm{T}}\mathbf{R}^{-1}(\mathbf{y} - \mathbf{G}\tilde{\boldsymbol{\beta}}) \tag{9}$$

where $\mathbf{g}_0$ is the vector of $g_j(\mathbf{x}_0)$ and $\mathbf{r}_0$ is the vector of $C(\mathbf{x}_0,\mathbf{x}^{(i)})$ and $\tilde{\boldsymbol{\beta}} = (\mathbf{G}^{\mathrm{T}}\mathbf{R}^{-1}\mathbf{G})^{-1}\mathbf{G}^{\mathrm{T}}\mathbf{R}^{-1}\mathbf{y}$. The mean square error is given by

$$\begin{aligned} s^2(\mathbf{x}_0) = \sigma^2(1 - \mathbf{r}_0^{\mathrm{T}}\mathbf{R}^{-1}\mathbf{r}_0 \\ + (\mathbf{g}_0 - \mathbf{G}^{\mathrm{T}}\mathbf{R}^{-1}\mathbf{r}_0)^{\mathrm{T}}(\mathbf{G}^{\mathrm{T}}\mathbf{R}^{-1}\mathbf{G})^{-1}(\mathbf{g}_0 - \mathbf{G}^{\mathrm{T}}\mathbf{R}^{-1}\mathbf{r}_0)) \end{aligned} \tag{10}$$

Efficient Global Optimization Algorithm. The basic idea of the EGO algorithm consists of the creation of a Kriging surrogate model from an initial DoE which is updated at each iteration of the algorithm by adding a new point in the DoE [23]. The algorithm ends when a stop criterion is reached. The global work-flow of the method is given in Fig. 7. Thus, the point added is based on the expected improvement (EI) criterion and is chosen in order to increase the knowledge in the area of the design space where the minimum of the objective function can be located, but also to explore areas where no knowledge is available. This is performed by using the metamodel created at the current step. The stop criterion is often based on a maximum number of iterations.

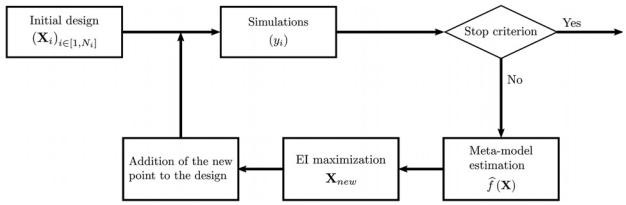

Fig. 7 Algorithm EGO scheme

A modified EI proposed by Raponi et al. [22] is considered for this study. It is similar to the classical EI when the design corresponding to the points $\mathbf{x}$ is feasible (the connectivity between the components is ensured) and is penalized when the design is not feasible (i.e., when the components are not connected). Hence, at the point $\mathbf{x}$, the EI is defined as [22,23,38]

$$EI[\mathbf{x}] = \begin{cases} \left(y_{\min} - \hat{f}(\mathbf{x})\right)\Phi\left(\dfrac{y_{\min} - \hat{f}(\mathbf{x})}{\hat{s}(\mathbf{x})}\right) + \hat{s}(\mathbf{x})\phi\left(\dfrac{y_{\min} - \hat{f}(\mathbf{x})}{\hat{s}(\mathbf{x})}\right) \\ \qquad\qquad \text{if feasible design and } \hat{s}(\mathbf{x}) \neq 0 \\ 0\,, \qquad\qquad \text{if feasible design and } \hat{s}(\mathbf{x}) = 0 \\ -P * \gamma, \qquad\qquad \text{if infeasible design} \end{cases} \tag{11}$$

where $y_{\min}$ is the current minimum, Φ is the Gaussian cumulative distribution function, and ϕ is the Gaussian probability density function, P is the minimum gap distance between the components, and $\gamma \in \mathbb{R}^{+*}$ is the penalization factor (equal to 1000 here). The new point $\mathbf{x}_{\text{new}}$ is the solution that maximizes the EI. This optimization problem is solved by using a genetic algorithm [39].

Updating Limit Conditions. For each point initially in the DoE and at each new point added during the process, a new damper geometry is described through the vector $\mathbf{x}$. Hence, the loading and the contact are also impacted and must be updated for each damper geometry. From the mass evolution of the damper, the centrifugal loading C_F also evolves, and so, the contact pressure and the contact stiffnesses are also impacted. The updating of the contact pressure is done by considering the new value of the

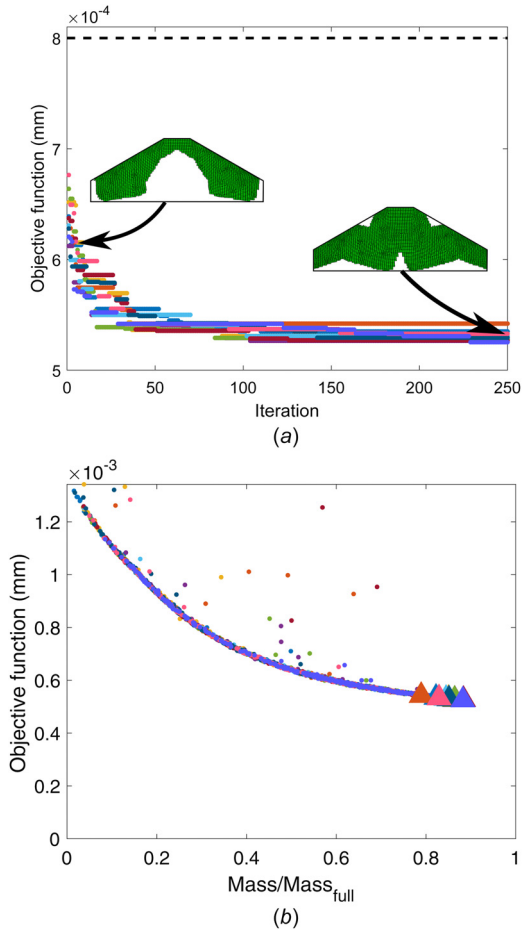

Fig. 8 (*a*) Evolution of the objective function (i.e., max of displacements at blades tips) and (*b*) objective function versus the normalized mass of the damper for all the different configurations tested during the algorithm. (*a*) One color corresponds to one DoE—(– – –) full damper (reference)—initial and final geometries for one DoE and (*b*) one color corresponds to one DoE—(△) final solution.

centrifugal loading C_F that depends on the damper mass and also by considering the new contact area A that is related to the damper geometry in Eq. (1).

Moreover, the contact stiffness depends on the contact loading, and so, they are also updated at each iteration by keeping the constant ratio [40]

$$\frac{k^{(1)}}{\sigma^{(1)}} = \frac{k^{(i)}}{\sigma^{(i)}} \tag{12}$$

where $k^{(i)}$ is the contact stiffness and $\sigma^{(i)}$ the contact pressure at the iteration i. As a reminder, $k = k_t = k_n$.

Summary of the Global Process. Finally, the global layout of the methodology can be described as follows. First, the initialization part can be decomposed as follows:

- Initialization/step 1: a LHS is generated for the initial input points. Only the geometries that are connected are retained [22].
- Initialization/step 2: the LSF corresponding to the design point is constructed and mapped on the initial damper mesh. The final damper mesh is created by eliminating the void elements.
- Initialization/step 3: for each damper geometry, the nonlinear dynamic response of both the platform and the damper is determined with the MHBM where the contact pressure and contact stiffness have been updated. The excitation amplitude is constant and equal to 1×10^{-3} N. The maximum of displacements at the blades tips over the frequency range [200, 400] Hz is retained as the evaluation of the objective function.

and the general optimization loop can be decomposed as follows:

- Loop/step 1: from the DoE, a surrogate model is generated.
- Loop/step 2: from the surrogate model, the EI is maximized and the new point is added to the design.
- Loop/step 3: for this point (i.e., new geometry), the objective function is determined (steps 2 and 3 of the initialization).

The loop is repeated until the stop criterion is reached. Concerning some practical aspects, in this study, the global work-flow is piloted using MATLAB. The package DiceKriging [38] on R is used for the creation of the different Kriging metamodels. A kernel Matérn 5/2 is used, and the regression function is polynomial of order 0.

Application

The methodology presented previously is then applied to optimize the topology of the damper. Seven components are used to describe the geometry of the damper, as shown in Fig. 6, which would represent 35 optimization parameters. In order to reduce

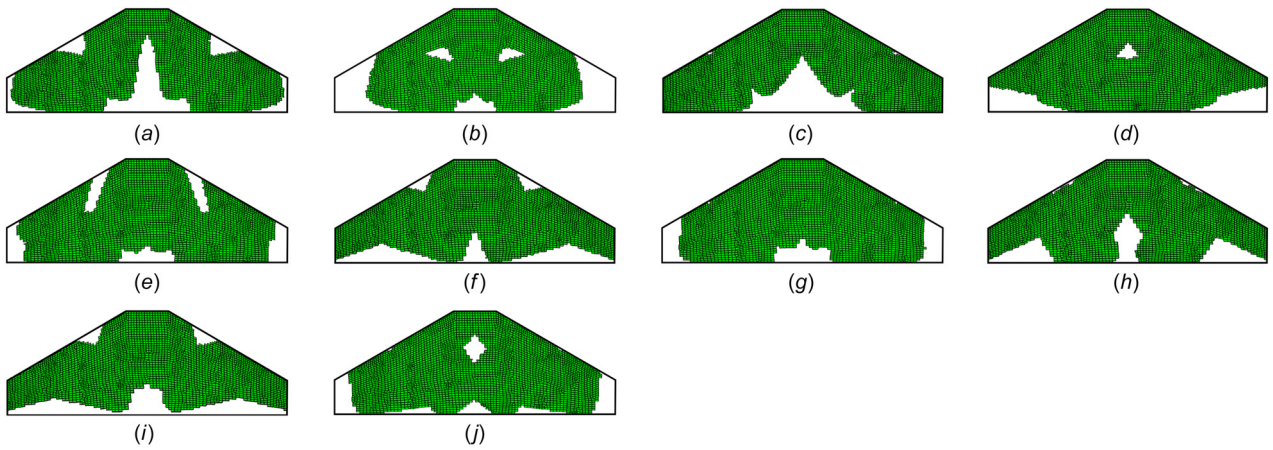

Fig. 9 Damper geometries obtained from the different DoE: (*a*) damper geometry from DoE1, (*b*) damper geometry from DoE2, (*c*) damper geometry from DoE3, (*d*) damper geometry from DoE4, (*e*) damper geometry from DoE5, (*f*) damper geometry from DoE6, (*g*) damper geometry from DoE7, (*h*) damper geometry from DoE8, (*i*) damper geometry from DoE9, and (*j*) damper geometry from DoE10

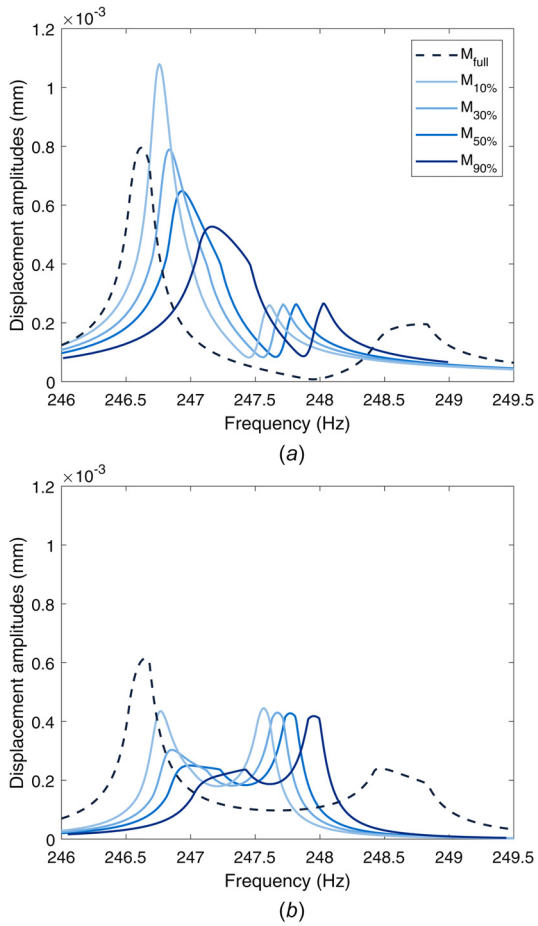

Fig. 10 Displacements amplitudes at blades tip nodes for different masses of damper: full damper, $M = 90\%M_{\text{full}}$, $M = 50\%M_{\text{full}}$, $M = 30\%M_{\text{full}}$, $M = 10\%M_{\text{full}}$. (*a*) Left blade (*b*) and right blade.

this number of parameters, some assumptions are done. First, a component is assumed to be horizontal at the top of the design space and aims to seal the platforms. This constraint comes from the fact that the primary function of a UPD is to seal the platforms to ensure the aerodynamic efficiency. Second, the damper is supposed to be symmetric. Finally, one component has its center position imposed to always have a contact between the damper and the platforms. This restriction ensures just a feasible design. Thanks to these restrictions, the final optimization problem is composed of 14 parameters. As a reminder, the excitation amplitude remains constant and is equal to 1×10^{-3} N.

Results. To ensure the validity and the robustness of the method, ten initial DoE are created and ten simulations are launched. In each case, an initial LHS of 10^5 points is generated, and only the feasible geometries are kept (i.e., no connectivity issue). Depending on the case, it represents $[65, 51, 65, 62, 62, 56, 82, 61, 62, 81]$ initial learning points for the ten cases. In order to get reasonable computation time, a maximum of 250 iterations is chosen. Hence, the evolution of the current minimum at each iteration for the ten cases is given in Fig. 8(*a*), where each color corresponds to one case. At the first iteration, the minimum is the one observed in the initial DoE, depending on the case it is included between 6 and 6.8×10^{-4} mm. Then, the evolution of the minima is quite similar for all cases. First, the decrease in the minimum is fast. Indeed, in about 40 iterations, all the minima are below 5.5×10^{-4} mm. After 40 iterations, the decrease becomes slower and stabilizes around 150 iterations. For all cases, the algorithm converges to a solution from 5.3 to 5.4×10^{-4} mm. It is worth reminding that for the full damper, the maximum level of amplitudes is equal to 8×10^{-4} mm. Hence, the algorithm identifies here ten solutions that are 30% more efficient than the original one.

As explained previously, no constraint on the volume is considered in this application. It may sound peculiar since the first objective of topological optimization is to reduce the weight of the structure. In this case, the most important objective is to achieve better design. Considering a constraint on the weight could lead to miss some interesting layouts. However, it is still an interesting argument to consider a solution instead of another one. Hence, Fig. 8(*b*) represents the maximum of displacements versus the normalized mass for all the configurations tested with the ten cases. It appears that almost all the configurations tested are located on a front. It shows also that by minimizing the maximum of displacements, the mass increases, i.e., the two functions are antagonist. The last configuration identified in each case, i.e., the current minimum at the iteration 250, is represented on the graph with a triangle. They are all located in the same part of the graph and so have similar masses.

The ten final configurations are given in Fig. 9. The green part corresponds to the mesh associated with each geometry, and the borders of the design space are reminded. It can be seen that the geometries are all different. Indeed, some have holes inside the structure (see in Figs. 9(*b*), 9(*d*), and 9(*j*)), and some cut the contact surface into two parts (see in Figs. 9(*a*), 9(*e*), 9(*f*), and 9(*i*)). However, some geometries look similar and some groups can be done. For example, geometries of Figs. 9(*a*), 9(*f*), and 9(*i*) have

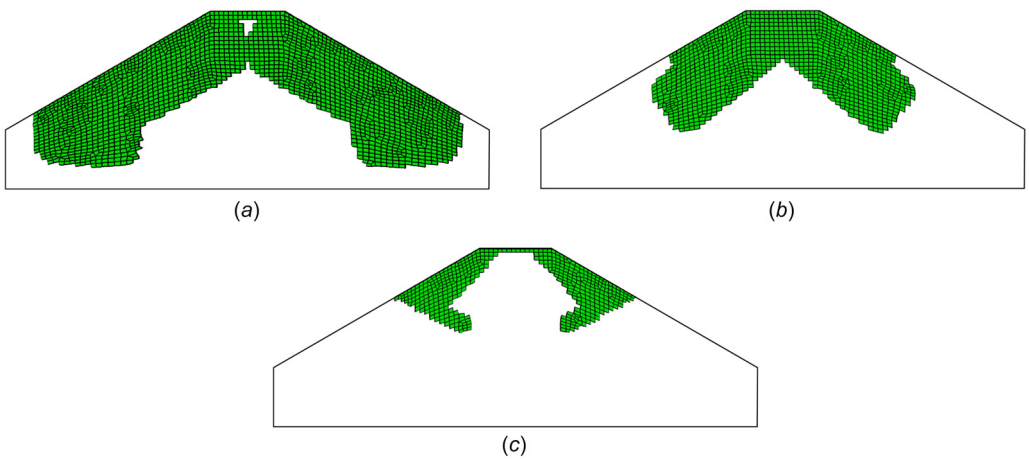

Fig. 11 Lighter geometries of damper observed during the optimization: (*a*) $M = 0.5M_{\text{full}}$, (*b*) $M = 0.3M_{\text{full}}$, and (*c*) $M = 0.1M_{\text{full}}$

very similar layouts. It appears that the FRF of each configuration is almost identical so only one of them is represented in the following. The FRF is given in Fig. 10(*a*) for the tip point on the left blade and in Fig. 10(*b*) for the right blade. The FRF corresponding to the solutions of the optimization is in dark blue, and the FRF of the full damper is represented with the black dotted line. They are given only for the horizontal displacement. In the initial case, the first peak was located at 246.6 Hz and the second at 248.8 Hz. The FRFs of the optimized geometries have a first peak shifted on the right (new peak at 247.2 Hz), whereas the second one is shifted on the left (new peak at 248 Hz). The same phenomenon appears on the second node: the first peak is shifted from 246.7 Hz to 247.5 Hz and the second from 248.5 Hz to 248 Hz. Moreover, in the initial case, the FRF of the two DOF was similar: the first peak has the largest amplitude and the second the smaller, whereas after optimization, for the second DOF, the second peak is the one with the largest amplitude.

In order to observe the efficiency of lighter dampers, the FRF of other geometries tested during the optimization process is considered. Geometries with a mass equal to 50%, 30%, and 10% of the total mass M_{full} are considered. One of each case is represented in Fig. 11. As previously, for one mass, all the FRF are extremely similar; hence, only one FRF is retained in each case for the comparison. The different FRF are represented in Fig. 10. The black dashed line corresponds to the initial case (full damper). For the first DOF, a decrease in the mass tends to increase the amplitude of the first peak: 1.1×10^{-4} mm of amplitude if $M = 0.1M_{\text{full}}$ and 0.54×10^{-4} mm if $M = 0.9M_{\text{full}}$. For the second peak, a lighter damper tends to decrease slightly the amplitudes. Moreover, the all FRF tend to be shifted on the left when the damper is lighter. Considering the second DOF (see in Fig. 10(*b*)), when the damper has a mass M equal to $0.1M_{\text{full}}$, the two peaks have similar amplitudes. The increase in the mass tends to reduce the amplitude of the first peak, whereas the amplitude of the second peak remains sensibly constant. As for the other DOF, the FRF is shifted on the right when the mass increases.

Conclusion

In this study, TO is applied to optimize nonlinear vibrations in the presence of a friction interface, which is completely new for the community from authors knowledge. A simple 2D model composed of two blades and a UPD, where the topology of the damper is optimized, is used as a test case. The TO method is based on the MMC framework to parameterize the LSF that describes the geometry of the system. A Kriging method together with the EGO algorithm is used as optimization process. This study was aimed to investigate the capacity of the MMC framework coupled with a global optimization algorithm to perform TO for nonlinear vibrations in a presence of a friction interface. Ten simulations based on different DoE are launched to verify the validity and the robustness of the approach. The results show a large variety of UPD geometries, but they all have very similar effectiveness and almost identical nonlinear dynamic response. The optimized geometries lead to a reduction of about 30% of the nonlinear vibration levels of the structure compared to the case with the full damper. The results obtained in the study tend to show the promising aspect of using the MMC framework coupled with EGO algorithm for TO of UPD. Nevertheless, a deeper investigation must be conducted to take into consideration different mechanical constraints, as the stress, to obtain more realistic layouts that can tolerate the operating conditions.

Acknowledgment

The authors thank Rolls-Royce plc and the EPSRC for the support under the Prosperity Partnership Grant "Cornerstone: Mechanical Engineering Science to Enable Aero Propulsion Futures," Grant No. EP/R004951/1.

Funding Data

- Engineering and Physical Sciences Research Council (Grant No. EP/R004951/1; Funder ID: 10.13039/501100000266).

Nomenclature

AFT = alternate frequency/time
DoE = design of experiments
DOF = degree-of-freedom
EGO = efficient global optimization
FRF = frequency response function
LHS = Latin hypercube sampling
LSF = level-set function
MHBM = multiharmonic balance method
MMC = moving morphable components
TO = topological optimization
UPD = underplatform damper

References

[1] Krack, M., Salles, L., and Thouverez, F., 2017, "Vibration Prediction of Bladed Disks Coupled by Friction Joints," Arch. Comput. Methods Eng., **24**(3), pp. 589–636.
[2] Petrov, E., and Ewins, D., 2004, "State-of-the-Art Dynamic Analysis for Non-Linear Gas Turbine Structures," Proc. Inst. Mech. Eng., Part G, **218**(3), pp. 199–211.
[3] Cowles, B., 1996, "High Cycle Fatigue in Aircraft Gas Turbines—An Industry Perspective," Int. J. Fract., **80**(2–3), pp. 147–163.
[4] Gaul, L., and Nitsche, R., 2001, "The Role of Friction in Mechanical Joints," ASME Appl. Mech. Rev., **54**(2), pp. 93–106.
[5] Feeny, B., Guran, A., Hinrichs, N., and Popp, K., 1998, "A Historical Review on Dry Friction and Stick-Slip Phenomena," ASME Appl. Mech. Rev., **51**(5), pp. 321–341.
[6] Griffin, J., 1990, "A Review of Friction Damping of Turbine Blade Vibration," Int. J. Turbo Jet Engines, **7**(3–4), pp. 297–308.
[7] Szwedowicz, J., Gibert, C., Sommer, T., and Kellerer, R., 2008, "Numerical and Experimental Damping Assessment of a Thin-Walled Friction Damper in the Rotating Setup With High Pressure Turbine Blades," ASME J. Eng. Gas Turbines Power, **130**(1), p. 012502.
[8] Sanliturk, K., Ewins, D., and Stanbridge, A., 2001, "Underplatform Dampers for Turbine Blades: Theoretical Modeling, Analysis, and Comparison With Experimental Data," ASME J. Eng. Gas Turbines Power, **123**(4), pp. 919–929.
[9] Sanliturk, K., Ewins, D., Elliott, R., and Green, J., 2001, "Friction Damper Optimization: Simulation of Rainbow Tests," ASME J. Eng. Gas Turbines Power, **123**(4), pp. 930–939.
[10] Petrov, E., and Ewins, D., 2007, "Advanced Modeling of Underplatform Friction Dampers for Analysis of Bladed Disk Vibration," ASME J. Turbomach., **129**(1), pp. 143–150.
[11] Panning, L., Sextro, W., and Popp, K., 2000, "Optimization of Interblade Friction Damper Design," ASME Paper No. 2000-GT-0541.
[12] Pesaresi, L., Salles, L., Jones, A., Green, J., and Schwingshackl, C., 2017, "Modelling the Nonlinear Behaviour of an Underplatform Damper Test Rig for Turbine Applications," Mech. Syst. Signal Process., **85**, pp. 662–679.
[13] Csaba, G., 1999, "Modelling of a Microslip Friction Damper Subjected to Translation and Rotation," ASME Paper No. 99-GT-149.
[14] Zucca, S., Botto, D., Gola, K., and Muzio, M., 2008, "Range of Variability in the Dynamics of Semi-Cylindrical Friction Dampers for Turbine Blades," ASME Paper No. GT2008-51058.
[15] Rozvany, G., and Zhou, M., 1993, "Layout and Generalized Shape Optimization by Iterative COC Methods," *Optimization of Large Structural Systems*, Springer, Dordrecht, The Netherlands, pp. 103–120.
[16] Eschenauer, H., and Olhoff, N., 2001, "Topology Optimization of Continuum Structures: A Review," ASME Appl. Mech. Rev., **54**(4), pp. 331–390.
[17] Bendsøe, M., 1989, "Optimal Shape Design as a Material Distribution Problem," Struct. Optim., **1**(4), pp. 193–202.
[18] Philip, M. B., and Kikuchi, N., 1988, "Generating Optimal Topologies in Structural Design Using a Homogenization Method," Comput. Methods Appl. Mech. Eng., **71**(2), pp. 197–224.
[19] van Dijk, N., Maute, K., Langelaar, M., and Keulen, F. V., 2013, "Level-Set Methods for Structural Topology Optimization: A Review," Struct. Multidiscip. Optim., **48**(3), pp. 437–472.
[20] Allaire, G., Jouve, F., and Toader, A.-M., 2004, "Structural Optimization Using Sensitivity Analysis and a Level-Set Method," J. Comput. Phys., **194**(1), pp. 363–393.
[21] Guo, X., Zhang, W., and Zhong, W., 2014, "Doing Topology Optimization Explicitly and Geometrically—A New Moving Morphable Components Based Framework," ASME J. Appl. Mech., **81**(8), p. 081009.
[22] Raponi, E., Bujny, M., Olhofer, M., Aulig, N., Boria, S., and Duddeck, F., 2019, "Kriging-Assisted Topology Optimization of Crash Structures," Comput. Methods Appl. Mech. Eng., **348**, pp. 730–752.
[23] Jones, D. R., Schonlau, M., and Welch, W. J., 1998, "Efficient Global Optimization of Expensive Black-Box Functions," J. Global Optim., **13**(4), pp. 455–492.
[24] Sun, J., Tian, Q., Hu, H., and Pedersen, N. L., 2019, "Topology Optimization for Eigenfrequencies of a Rotating Thin Plate Via Moving Morphable Components," J. Sound Vib., **448**, pp. 83–107.

[25] Bendsøe, M. P., and Díaz, A. R., 1994, "Optimization of Material Properties for Improved Frequency Response," Struct. Optim., **7**(1–2), pp. 138–140.
[26] Díaaz, A. R., and Kikuchi, N., 1992, "Solutions to Shape and Topology Eigenvalue Optimization Problems Using a Homogenization Method," Int. J. Numer. Methods Eng., **35**(7), pp. 1487–1502.
[27] Allaire, G., and Jouve, F., 2005, "A Level-Set Method for Vibration and Multiple Loads Structural Optimization," Comput. Methods Appl. Mech. Eng., **194**(30–33), pp. 3269–3290.
[28] Dou, S., and Jensen, J. S., 2015, "Optimization of Nonlinear Structural Resonance Using the Incremental Harmonic Balance Method," J. Sound Vib., **334**, pp. 239–254.
[29] Dou, S., Strachan, B. S., Shaw, S. W., and Jensen, J. S., 2015, "Structural Optimization for Nonlinear Dynamic Response," Philos. Trans. R. Soc. A, **373**(2051), p. 20140408.
[30] Myśliński, A., 2012, "Topology Optimization of Quasistatic Contact Problems," Int. J. Appl. Math. Comput. Sci., **22**(2), pp. 269–280.
[31] Strömberg, N., and Klarbring, A., 2010, "Topology Optimization of Structures in Unilateral Contact," Struct. Multidiscip. Optim., **41**(1), pp. 57–64.
[32] Maury, A., Allaire, G., and Jouve, F., 2017, "Shape Optimisation With the Level Set Method for Contact Problems in Linearised Elasticity," SMAI J. Comput. Math., **3**, pp. 249–292.
[33] Petrov, E., 2008, "Explicit Finite Element Models of Friction Dampers in Forced Response Analysis of Bladed Disks," ASME J. Eng. Gas Turbines Power, **130**(2), p. 022502.
[34] Petrov, E., 2011, "A High-Accuracy Model Reduction for Analysis of Nonlinear Vibrations in Structures With Contact Interfaces," ASME J. Eng. Gas Turbines Power, **133**(10), p. 102503.
[35] Cameron, R., and Martin, W., 1947, "The Orthogonal Development of Non-Linear Functionals in Series of Fourier-Hermite Functionals," Ann. Math., **48**(2), pp. 385–392.
[36] Challis, V., 2010, "A Discrete Level-Set Topology Optimization Code Written in Matlab," Struct. Multidiscip. Optim., **41**(3), pp. 453–464.
[37] Li, Z., Shi, T., and Xia, Q., 2017, "Eliminate Localized Eigenmodes in Level Set Based Topology Optimization for the Maximization of the First Eigenfrequency of Vibration," Adv. Eng. Software, **107**, pp. 59–70.
[38] Roustant, O., Ginsbourger, D., and Deville, Y., 2012, "Dicekriging, Diceoptim: Two R Packages for the Analysis of Computer Experiments by Kriging-Based Metamodeling and Optimization," J. Statistical Software, **51**(1), pp. 1–55.
[39] Goldberg, D., and Holland, J., 1988, "Genetic Algorithms and Machine Learning," Mach. Learn., **3**(2/3), pp. 95–99.
[40] Sextro, W., 2007, *Dynamical Contact Problems With Friction*, Springer, Berlin.